

# Adhesion of Ethylene–Styrene Copolymers to Polyethylene in Microlayers

V. Ronesi,<sup>1</sup> Y. W. Cheung,<sup>2</sup> A. Hiltner,<sup>1</sup> E. Baer<sup>1</sup>

<sup>1</sup>Department of Macromolecular Science and Center for Applied Polymer Research, Case Western Reserve University, Cleveland, Ohio 44106-7202

<sup>2</sup>The Dow Chemical Company, Polyolefins and Elastomers R & D, The Dow Chemical Company, Freeport, Texas 77541

Received 20 August 2002; accepted 22 September 2002

**ABSTRACT:** The effects of styrene content, layer thickness, and temperature on the adhesion of ethylene–styrene copolymers (ES) to low-density polyethylene (LDPE) were examined by measuring the delamination toughness of LDPE/ES microlayers in the T-peel test. Delamination toughness at ambient temperature decreased with increasing styrene content. A linear correlation between delamination toughness and styrene content in ES was observed. Extrapolation predicted that a copolymer with 72.5 wt % styrene would have no adhesion to LDPE. Experiments on microlayers with relatively thin (8–18  $\mu\text{m}$ ) ES layers demonstrated that delamination toughness was proportional to ES layer thickness. *In situ* observations of the damage zone showed stretching throughout the entire thickness of the ES layer. For higher adhesion systems, ES deformation occurred concurrently with localized stretching and crazing of

the LDPE layer at the interface. For two representative systems, the effect of temperature on delamination toughness was studied. Major transitions in delamination toughness and fracture mode were observed at the primary thermal transitions of the ES copolymer. The contribution by stretching of the ES layer to measured delamination toughness was approximated by relating the damage zone to the ES engineering stress–strain curve and was estimated to be about half. The remaining contribution to delamination toughness was assumed to be due to LDPE deformation in the damage zone. © 2003 Wiley Periodicals, Inc. *J Appl Polym Sci* 89: 153–162, 2003

**Key words:** ethylene copolymers; styrene copolymers; polyethylene; microlayers; delamination toughness

## INTRODUCTION

It is well known that polyethylene and polystyrene do not adhere to each other; however, to have useful blends or layered films of these two polymers, good adhesion is required. Copolymers of ethylene and styrene are ideal materials to compatibilize the component polymers and thus promote good adhesion. Recent commercial developments in advanced catalyst technology have allowed for efficient copolymerization of ethylene with styrene.<sup>1</sup> The ethylene–styrene (ES) copolymers exhibit a very broad range of structure and properties depending on styrene content. A classification scheme has been developed with three distinct categories based on structure–property relationships.<sup>1</sup> Copolymers with up to 50 wt % styrene are semicrystalline, and those materials in this category with low crystallinity exhibit rubbery behavior. Amorphous copolymers with more than 50 wt % styrene are separated into two other categories depending on the glass transition relative to ambient temperature. Amorphous copolymers with a glass transition tem-

perature ( $T_g$ ) less than ambient temperature are classified as amorphous rubbers and those with a higher  $T_g$  are classified as amorphous glassomers.

Microlayered systems with many alternating layers of two or more polymers can be thought of as one-dimensional blends. The layers can be readily controlled to thicknesses on similar size scales as domains in commercial blends. Therefore it is now possible to attempt to quantify the adhesion in an immiscible blend. Because the layers are relatively thin compared to an average adhesive layer, the effect of layer thickness or scale must be considered. For relatively brittle adhesives, an effect of layer thickness is usually small because of the inability to form a significant damage zone ahead of the crack tip.<sup>2,3</sup> In contrast, the measured adhesive fracture energy for tougher, rubbery adhesives is highly dependent on layer thickness because in this case a large damage zone can form prior to delamination.<sup>2,3</sup> Adhesive toughness usually increases with thickness because the development of the damage zone is less restricted. A maximum toughness is achieved when the layer thickness and the damage zone size are approximately equal. For rubbery adhesives, a transition from cohesive fracture in the damage zone to interfacial fracture between the adhesive and adherend is strongly affected by rate and temperature. Consequently, this transitional phenomenon,

Correspondence to: A. Hiltner (pah6@po.cwru.edu).  
Contract grant sponsor: Dow Chemical Co..

TABLE I  
Characterization of Resin Materials

Sample	Styrene content (wt %)	aPS (wt %)	$10^{-3} M_w$	$M_w/M_n$	$T_g$ (°C)	$T_m$ (°C)		Crystallinity (wt %)
						Onset	Peak	
ES30	30.3	0.4	180.5	2.7	-4	-16	61	18
ES40	39.5	1.2	183.1	2.3	-7	-18	31	6
ES60	59.7	2.3	255.0	2.5	16	—	—	—
ES68	68.4	5.8	282.2	2.2	31	—	—	—
LDPE	—	—	90.5	6.0	—	106	110	45

which depends on the viscoelastic properties of the individual polymers, strongly influences the adhesive toughness.<sup>2-4</sup>

In previous work, the adhesion of polycarbonate (PC) to poly(styrene-*co*-acrylonitrile) (SAN) was characterized by studying the effects of AN content, layer thickness, and certain viscoelastic parameters.<sup>5-7</sup> Maximum PC/SAN interfacial toughness was observed at about 20% AN, which successfully compared with several predictions of relative interfacial toughness based on the interaction parameter,  $\chi$ .<sup>7</sup> The SAN copolymer with 20% AN was used in all subsequent comparisons. For systems that had very thin SAN layers (0.5  $\mu\text{m}$ ) and relatively thick PC layers (5  $\mu\text{m}$ ), virtually no crazing occurred and brittle fracture was observed at the interface. The real interfacial toughness was independent of peel rate and temperature and observed to be 90 J/m<sup>2</sup> for all test conditions. With increasing SAN layer thickness, crazing occurred in front of the crack tip in the SAN layer and the size of the damage zone increased, resulting in a higher delamination toughness. For systems with thicker SAN layers, the real interfacial toughness was approached by either decreasing peel rate or increasing temperature, conditions that gradually suppressed SAN crazing. As expected, when virtually no SAN crazing occurred, the delamination toughness again decreased and leveled off to the real interfacial toughness of 90 J/m<sup>2</sup>. The observed transition from craze-dominated cohesive fracture to predominantly interfacial fracture correlated to the properties of bulk SAN.

In the present study, the adhesion of ethylene-styrene copolymers to polyethylene has been analyzed following the methodology of previous work. A range of ES copolymers was chosen to span the aforementioned classification scheme which was anticipated to give a diverse spectrum of adhesive properties. The properties of the adhesive layer which controls the delamination toughness were elucidated and correlated with the stability of the damage zone.

## EXPERIMENTAL

The ethylene-styrene copolymers used in this study were synthesized by INSITE™ technology (INSITE™

is a trademark of The Dow Chemical Co., Midland MI) and are described in Table I. Information on comonomer content, molecular weight, and molecular weight distribution were provided by the manufacturer. The copolymers, designated as ES followed by wt % styrene, have mostly random incorporation of styrene except that multiple head-to-tail styrene insertions do not occur. In all microlayered systems, a single low-density polyethylene (LDPE) was used, Dow LDPE (PE 526A,  $I_2 = 1.0 \text{ g } 10 \text{ min}^{-1}$ ), with a weight-average molecular weight of 90,500 and a molecular weight distribution ( $M_w/M_n$ ) of 6.0 as reported by the manufacturer.

Microlayer tapes with alternating layers of LDPE and ES were coextruded by using the layer-multiplying process described previously.<sup>8</sup> Tapes were coextruded about 2 mm thick and 10 mm wide with 33 alternating layers of LDPE and ES (17 LDPE layers and 16 ES layers). To ensure a constant thermal history and to avoid any processing temperature effects on adhesion, all microlayer systems were processed at the same temperatures. The LDPE extruder was 240°C; the ES extruder was 250°C, and the multipliers and exit die were at 245°C. Extruder feed ratios were varied to produce microlayers with different compositions and layer thicknesses as shown in Table II. The various microlayered materials were defined by measuring the average thickness of the five center layers in a conventional optical microscope (OM). For characterization of the bulk materials, pellets of ES and LDPE were also compression molded.

Delamination was carried out with the T-peel test (ASTM D 1876). To initiate crack propagation, speci-

TABLE II  
Microlayer Composition and Layer Thickness

Volume ratio (LDPE/ES)	Center layer thicknesses	
	LDPE ( $\mu\text{m}$ )	ES ( $\mu\text{m}$ )
LDPE/ES30	90/10	115 $\pm$ 15
	95/5	110 $\pm$ 15
LDPE/ES40	90/10	120 $\pm$ 20
	95/5	105 $\pm$ 15
LDPE/ES60	90/10	120 $\pm$ 20
	95/5	110 $\pm$ 15
LDPE/ES68	90/10	120 $\pm$ 20
	95/5	115 $\pm$ 10

mens about 6.5 mm wide were notched at one of the five center layers. Adhesion tests were conducted in either an Instron 1123 or an Instron 1122 at crosshead speeds ranging from 0.1 to 1000 mm/min. Tests at various temperatures between  $-70$  and  $90^\circ\text{C}$  were conducted at a peel rate of 10 mm/min. To examine the damage zone at the crack tip, *in situ* observations were made with a video camera attached to an Infinity telescopic lens.

The peeled fracture surfaces were analyzed in a scanning electron microscope (SEM, JEOL 840A). These surfaces were coated with 100 Å of gold. To study the damage zone in front of the crack tip during delamination at higher magnifications than was possible with a telescopic lens, peel specimens were loaded into a Hexland B164 tensile stage and inserted into the SEM. Polished peel specimens were coated on the edges with 50 Å of gold and tested at a peel rate of 0.2 mm/min. To determine surface composition, uncoated sections of the fracture surfaces were characterized with a Nicolet 870 Nexus FTIR spectrometer with micro-ATR.

To characterize the bulk properties of the component polymers, differential scanning calorimetry (DSC), dynamic mechanical thermal analysis (DMTA), and stress-strain experiments were performed. Melting temperature and crystallinity were measured by DSC with a heating rate of  $10^\circ\text{C}/\text{min}$ . An enthalpy of 290 J/g for the perfect polyethylene crystal was used to calculate wt % crystallinity. The  $T_g$  was measured by DMTA in tension at a frequency of 1 Hz. The  $T_g$  was taken at the maximum of the loss tangent peak. Stress-strain behavior in uniaxial tension was measured with ASTM 1708 microtensile specimens at various strain rates.

## RESULTS AND DISCUSSION

### Peel data at ambient temperature

Typical normalized peel curves at ambient temperature and peel rate of 10 mm/min for microlayers with ES30, ES40, and ES60 are shown in Figure 1. The load increased because of the formation of the damage zone and bending of the beam arms until the crack started to propagate in a continuous manner. At this relatively constant load ( $P$ ), the delamination toughness was calculated as  $G = 2P/W$  for a specimen of width  $W$ . The delamination toughness decreased with increasing styrene content by more than half and scaled approximately with ES layer thickness. This indicated that deformation occurred through the entire thickness of the ES layer.

The effect of peel rate ranging from 0.1 to 1000 mm/min is shown in Figure 2. The ES layer thickness effect continued to be observed and showed how viscoelastic properties of ES and LDPE significantly af-

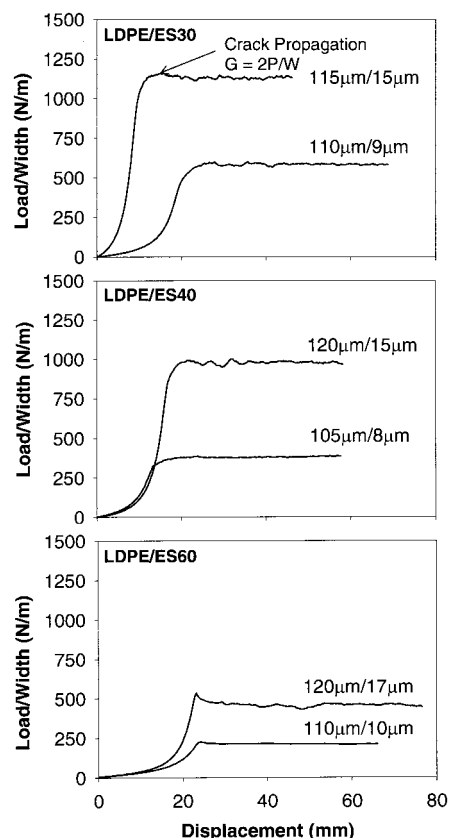


**Figure 1** Representative peel curves of (a) LDPE/ES30, (b) LDPE/ES40, and (c) LDPE/ES60 at ambient temperature and a peel rate of 10 mm/min. LDPE/ES layer thicknesses are indicated with peel curves.

ected  $G$ . For all systems, the delamination toughness increased about a factor of 2 over four decades of rate. A 25% increase in  $G$  at low rates for LDPE/ES60 was due to a change in delamination mechanism from interfacial to cohesive failure.

Unlike the other systems, LDPE/ES68 microlayers exhibited discontinuous crack propagation [Fig. 3(a)]. Delamination toughness was taken as the average of all maxima in the peel curves.<sup>9</sup> As expected, this system with the highest styrene content exhibited the lowest adhesion to LDPE. Because the glass transition of ES68 is around ambient temperature ( $31^\circ\text{C}$ ), this system was very sensitive to rate, as shown in Figure 3(b). A detailed description of the discontinuous peel mechanism and large rate effect is discussed in the next section.

The effect of styrene content on adhesion is shown in Figure 4 as delamination toughness normalized to ES layer thickness ( $h$ ),  $G_0 = G/h$ . The normalization clearly demonstrates that  $G$  scales with ES layer thickness. For the ES copolymers studied, a linear correlation between  $G$  and wt % styrene in ES was observed. Extrapolation to  $0 \text{ J}/\text{m}^2$  indicated no adhesion between LDPE and ES for a copolymer with 72.5 wt % styrene. This approximation

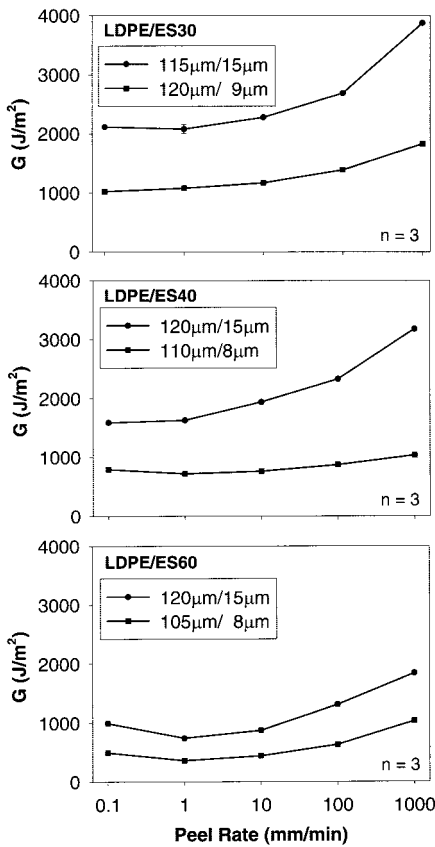


**Figure 2** Effect of peel rate on delamination toughness at ambient temperature of (a) LDPE/ES30, (b) LDPE/ES40, and (c) LDPE/ES60.

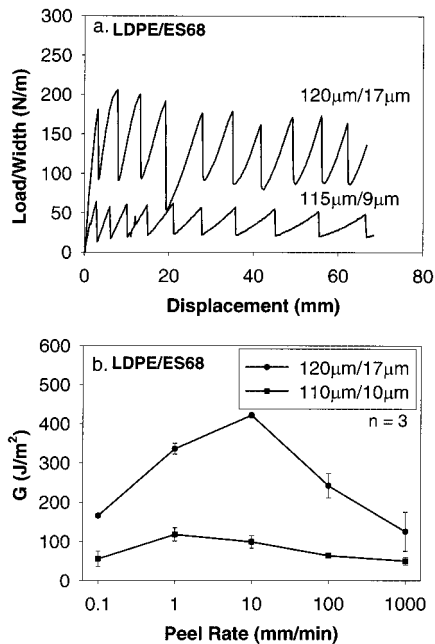


**Figure 3** (a) Representative peel curves of LDPE/ES68 at 10 mm/min and (b) effect of peel rate on delamination toughness at ambient temperature.

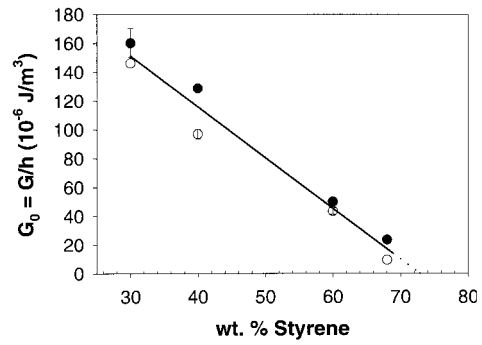


**Figure 4** Effect of styrene content on delamination toughness normalized to ES layer thickness at ambient temperature and peel rate of 10 mm/min. Closed circles represent 90/10 systems; open circles represent 95/5 systems. Dotted line is from extrapolation.

is close to the maximum styrene incorporation in ES copolymers of 80 wt % (50 mol %).

**Fracture mechanisms at ambient temperature**

To observe the crack tip region, specimens were loaded into a SEM tensile stage. Under a peel rate of 0.2 mm/min, the stable damage zone was observed. Figure 5 compares the damage zones of two systems, LDPE/ES30 (115/15 µm) and LDPE/ES40 (120/15 µm) with delamination toughness values of 2100 and 1800 J/m<sup>2</sup>, respectively. Bulk stretching of the center ES30 and ES40 layers to a draw ratio of 6.25 and 10.5,

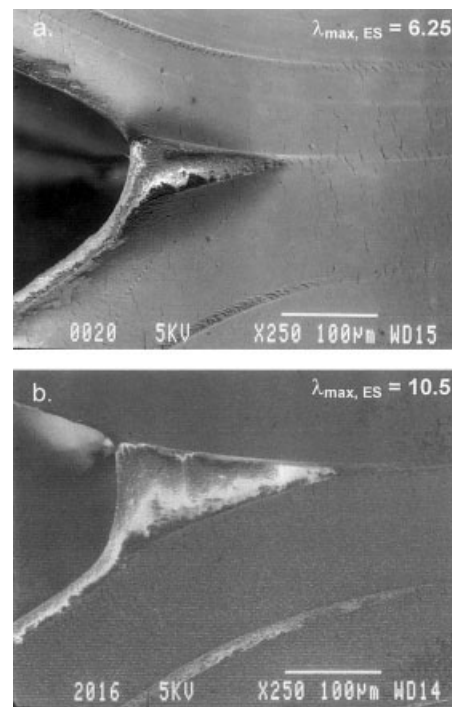


**Figure 5** Scanning electron micrographs from an *in situ* peel test of (a) LDPE/ES30 (115/15 µm) and (b) LDPE/ES40 (120/15 µm).

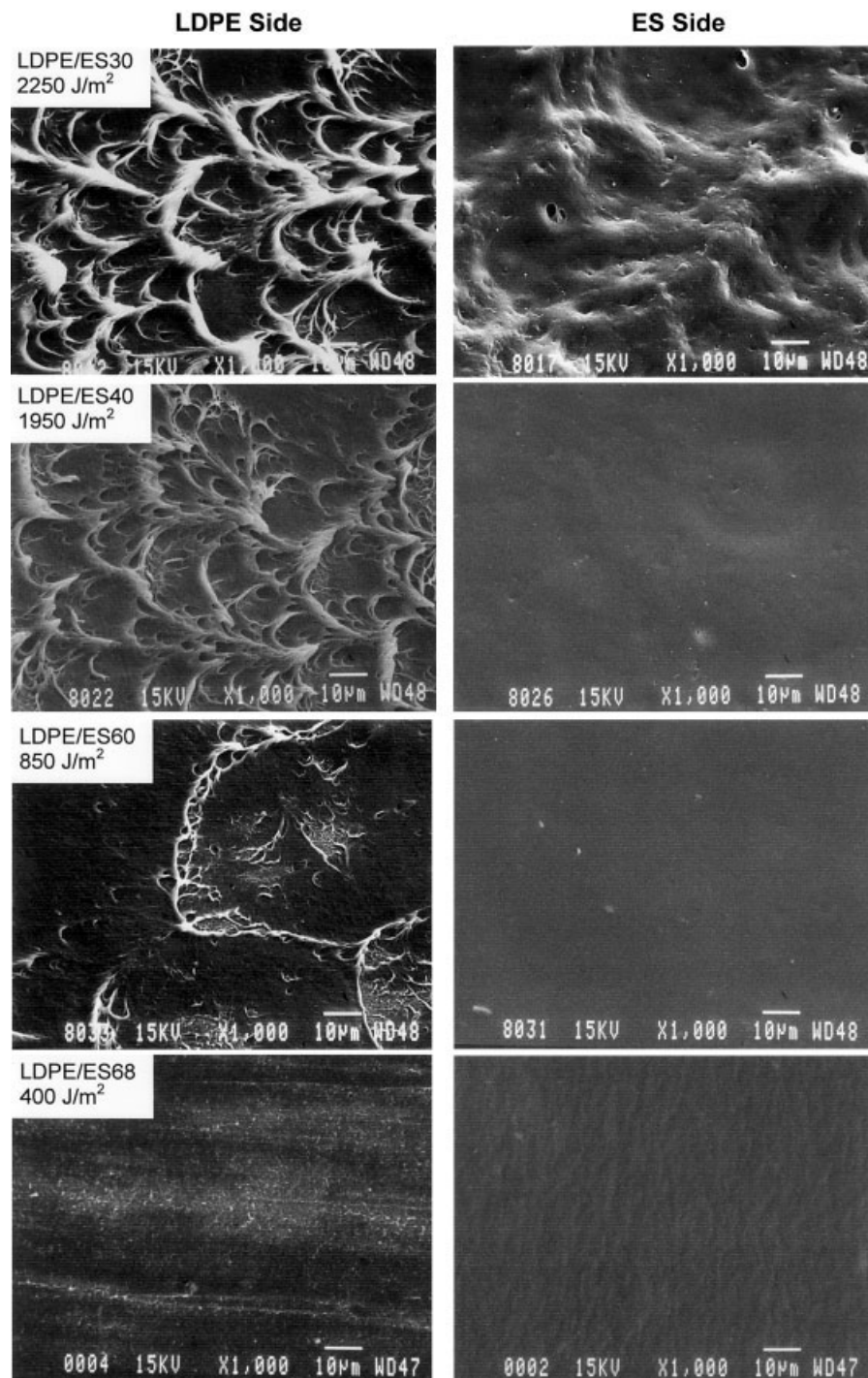


**Figure 6** Scanning electron micrographs of fracture surfaces for all LDPE/ES (90/10) systems at 10 mm/min and ambient temperature. The crack propagated from left to right.

respectively, and localized stretching of the LDPE layer at the interface were observed. These observations confirmed that there was deformation through the entire thickness of the ES layer and established why a factor of 2 difference in delamination toughness was observed. In addition, the contribution of polyethylene deformation was also determined.

To further elucidate the delamination mechanism, the peel fracture surfaces were examined in the SEM.

In Figure 6, the opposite fracture surfaces of all four systems with a 90/10 composition at a peel rate of 10 mm/min are shown. Examination of the fracture surfaces of LDPE/ES30 (115/15  $\mu\text{m}$ ,  $G = 2250 \text{ J/m}^2$ ) revealed a porous texture consisting of fractured fibrils on the LDPE side and on the ES30 side a rugged texture whose hills and valleys corresponded to imprints from the LDPE craze. FTIR micro-ATR analysis on the peel fracture surfaces confirmed that no ES30

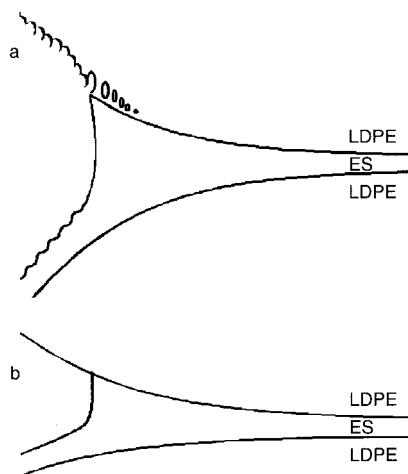


**Figure 7** Schematic representation of delamination failure mechanism for (a) high adhesion, LDPE/ES30, and LDPE/ES40 and (b) low adhesion, LDPE/ES60, and LDPE/ES68.

was transferred to the LDPE side. Similarly, LDPE/ES40 ( $120/15 \mu\text{m}$ ,  $G = 1950 \text{ J/m}^2$ ) exhibited the same polyethylene crazes but with significantly less permanent deformation on the ES40 side. For these two high adhesion systems ( $G > 1000 \text{ J/m}^2$ ), interfacial failure was accompanied by bulk stretching and subsequent recovery of the ES layer and concurrent surface cavitation and crazing of the LDPE layer [Fig. 7(a)].

For low adhesion systems ( $G < 1000 \text{ J/m}^2$ ), LDPE/ES60 and LDPE/ES68, much less damage appeared on the LDPE side, and the ES side appeared to have no damage. However, a layer thickness effect was still observed for these two systems, and it was therefore evident that deformation still occurred through the entire thickness of the ES layer. The delamination mechanism for the lower adhesion systems was thus interfacial failure accompanied only by small bulk stretching of the ES layer and its subsequent recovery after being peeled apart.

For LDPE/ES68, the damage zone consisted of stretching of the ES68 layer but the observed discontinuous crack propagation was more complicated. The stepwise crack propagation occurred because of a competition between the interfacial strength and the stored elastic energy in the beam arms. Stored elastic energy was either absorbed by the damage zone (stretching of the ES layer) or dissipated by propagating the crack. In this lowest adhesion system, it took more energy to bend the beam arms than to separate the interface. There was insufficient damage zone formation to absorb the stored elastic energy and therefore the crack jumped. The crack ran until there was not enough elastic energy to sustain further growth of the crack. As the crack was reopened, the process repeated itself along the length of the sample, resulting in the observed steps.

Stepwise crack propagation is usually indicative of transitional behavior. The transition here is the ES68

glass transition which is around ambient temperature ( $T_g = 31^\circ\text{C}$ ). This copolymer, characterized as a glass-tomer, exhibits glassy behavior at fast rates and rubbery behavior at slow rates.<sup>10</sup> As a result, this system was very sensitive to peel rate at ambient temperature, as shown in Figure 3(b). At lower rates, ES68 was rubbery and the delamination toughness decreased. Therefore, the softer material could form a large enough damage zone to prevent the crack from jumping. Thus, continuous crack growth was observed in LDPE/ES68 ( $120/17 \mu\text{m}$ ) at peel rates of 0.1 and 1 mm/min. In LDPE/ES68 ( $110/9 \mu\text{m}$ ), stepwise propagation was observed at all rates because the ES layer was too thin to absorb enough of the stored elastic energy in the beam arms.

### Effect of temperature

The effect of temperature on delamination toughness and peel mechanism was studied for LDPE/ES30 and LDPE/ES68. In these temperature experiments, the temperature range studied was significantly above the LDPE  $T_g$  (about  $-70^\circ\text{C}$ ) and below its melting temperature ( $110^\circ\text{C}$ ). Therefore, it was expected that changes in delamination toughness were primarily due to thermal transitions in ES30 and ES68.

The dependence of delamination toughness on temperature for LDPE/ES30 is shown in Figure 8(a), and major thermal transitions of glass transition and melting for ES30 are shown in Figure 8(b). Below  $T_g$ , ES30 became rigid and was no longer easily deformed. As a result, peel tests at temperatures below  $-10^\circ\text{C}$  were not successful because of the very high adhesion between ES30 and LDPE. During the experiment, the beam arms either yielded or broke before the crack could propagate.

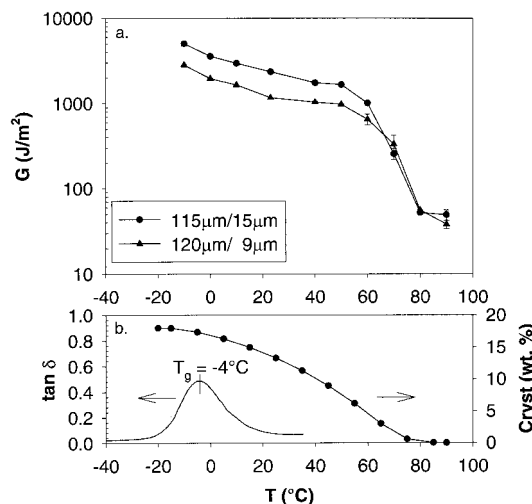


**Figure 8** (a) Effect of temperature on delamination toughness of LDPE/ES30. (b) Corresponding glass transition (DMTA) and crystallinity (DSC) for ES30.

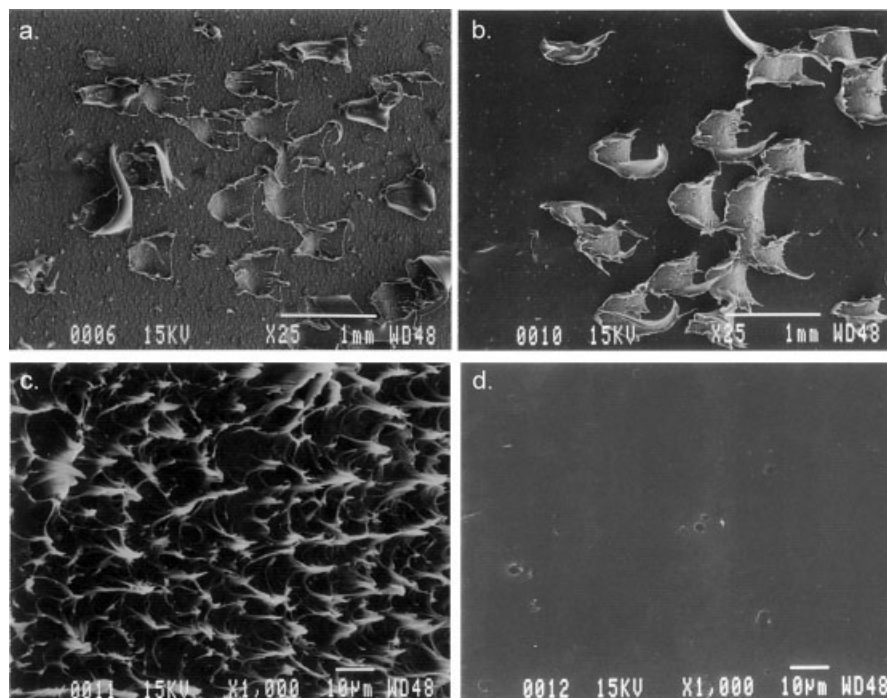


**Figure 9** Scanning electron micrographs of opposite fracture surfaces of LDPE/ES30 (115/15  $\mu\text{m}$ ) at  $-10^\circ\text{C}$ : (a) LDPE side, (b) ES30 side. Higher magnification micrographs of ES fracture surfaces; (c) chunks, (d) smooth. The crack propagated from left to right.

At  $-10^\circ\text{C}$  ( $G = 5000 \text{ J/m}^2$ ), delamination was stable but did not exhibit interfacial failure as was observed for this system at ambient temperature. Cohesive failure occurred in the LDPE layer. From SEM analysis of the fracture surfaces, large chunks were observed on opposite peel fracture surfaces [Fig. 9(a,b)]. Upon examination at a higher magnification on the ES30 fracture surface, two distinct textures were observed—LDPE crazes and smooth ES30 [Fig. 9(c,d)]. This was also confirmed by FTIR with micro-ATR analysis of fracture surfaces.

With increasing temperature through the ES30 glass transition and melting region,  $G$  decreased due to softening of the ES30 layer. From 0 to  $60^\circ\text{C}$ , no evidence of cohesive failure was observed on the

fracture surfaces. In addition, a layer thickness effect persisted, indicating that deformation occurred through the entire thickness of the ES layer. It was assumed that the damage zone was similar to that in Figure 7(a).

With increasing temperature through the ES30 melting point ( $61^\circ\text{C}$ ),  $G$  decreased by a factor of 10 and the layer thickness effect was no longer observed. In SEM micrographs of LDPE/ES30 peel surfaces at  $70^\circ\text{C}$  in Figure 10, ES30 was observed on both surfaces as whitened ribbons parallel to crack growth. The strength of the ES30 had decreased to such a degree that the interfacial strength was greater than the cohesive strength, and it was easier for the crack to run through the ES30 layer rather than along the interface.

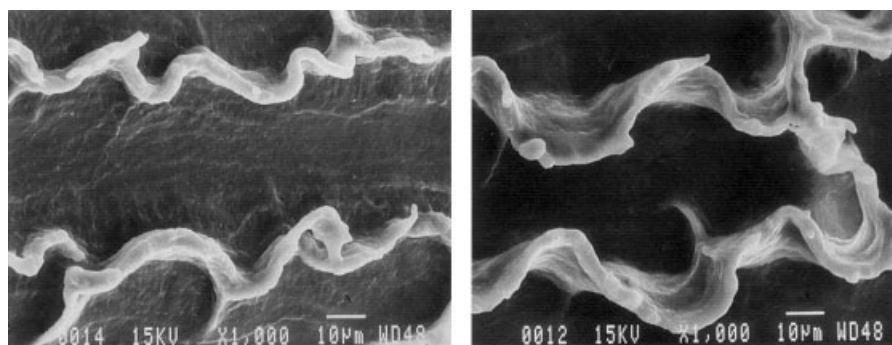


**Figure 10** Scanning electron micrographs of opposite fracture surfaces of LDPE/ES30 (115/15  $\mu\text{m}$ ) at  $70^\circ\text{C}$ . The crack propagated from left to right.

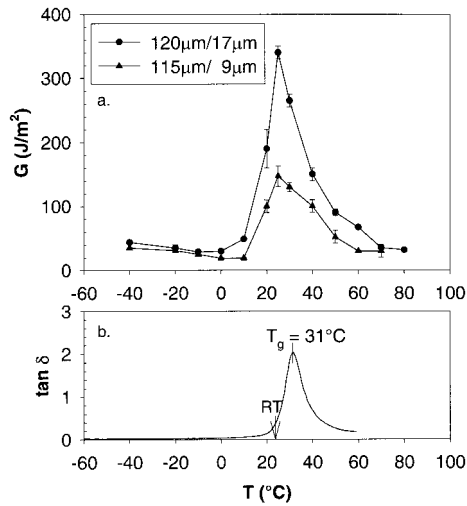


**Figure 11** (a) Effect of temperature on delamination toughness of LDPE/ES68. (b) Corresponding glass transition (DMTA) for ES68.

This was confirmed by examination of the fracture surfaces with FTIR-ATR analysis.

It is common for the failure mode in rubbery polymer adhesives to change from interfacial to cohesive as the temperature is increased.<sup>2,3</sup> A sharp drop in peel force with increased temperature is also typically observed. Gent et al. explained this behavior by attributing the interfacial fracture to the rubberlike state ( $>T_{gr} < T_m$ ) of the adhesive and the cohesive fracture to the liquidlike state ( $>T_m$ ).<sup>4</sup> Upon peeling, a sufficiently softened adhesive under sufficiently large forces cavitates before the crack propagates. The crack runs through the cavities, resulting in cohesive failure through the adhesive layer. Similarly, the transition from interfacial to cohesive failure at 70°C for LDPE/ES30 was due to the transition in ES30 from the rubberlike state to the liquidlike state.

The effect of temperature on the delamination toughness of the lowest adhesion system LDPE/ES68 is shown in Figure 11(a). At temperatures below the ES68  $T_{gr}$ , no layer thickness effect was observed due to the inability of ES68 to plastically deform and therefore no damage zone could develop, a mechanism similar to that of brittle adhesives. Discontinuous crack propagation occurred during peeling for both layer thicknesses at all low temperatures due to the very low interfacial adhesion relative to the bending of the beam arms. A delamination toughness of about 30 J/m<sup>2</sup> was observed and represents the true interfacial strength of ES68 to LDPE because there was no damage zone contribution to  $G$ . When the temperature was increased through the ES68  $T_{gr}$ , delamination toughness increased by a factor of 10 and the layer thickness effect was observed, indicating the formation of a damage zone. A maximum in  $G$  was observed at the glass transition of ES68 [Fig. 11(b)], a peak not ob-

served in LDPE/ES30 because peel experiments could not be successfully performed at temperatures through the entire glass transition of ES30. The peak corresponded to that found in previous experiments with peel rate [Fig. 3(b)].

A maximum in  $G$  is commonly observed in studies involving rate and temperature effects on peel measurements because at the glass transition, the maximum amount of energy is required for plastic deformation.<sup>4</sup> A layer thickness effect was observed within and above the ES68 glass transition up to 70°C, at which point ES68 had softened to such a degree that beam arm bending was the only contribution to  $G$ . Delamination toughness decreased with increasing temperature by a factor of 10. In contrast to LDPE/ES30, LDPE/ES68 did not exhibit cohesive failure at the chosen elevated temperatures because of the low interfacial adhesion.

#### Quantitative interpretation of delamination toughness

For LDPE/ES30 (115/15 µm), a quantitative description of ES30 bulk stretching for ambient temperature delamination was attempted by relating the ES30 stretching in the damage zone to its engineering stress-strain curve. From *in situ* SEM and OM observations, both the maximum draw ratio of the ES layer at the front of the crack tip ( $\lambda_{max}$ ) and the length of the damage zone ( $a$ ) were determined (Fig. 12). These measurements were made on the basis of the assumption that the damage zone at the edge of the peel specimen was very similar to that at the center, which was confirmed by measuring delamination toughness on both wide and narrow peel specimens. The results showed that sample width made no significant difference in measured  $G$  values, and therefore, the applied approach was validated.

From  $\lambda_{max}$  and  $a$ , the engineering strain rate ( $\dot{\epsilon}$ ) of the adhesive in the damage zone was calculated as:

$$\dot{\epsilon} = \frac{\text{strain}}{\text{time}} = (\lambda_{max} - 1) \left( \frac{\text{peel rate}}{2a} \right) \quad (1)$$

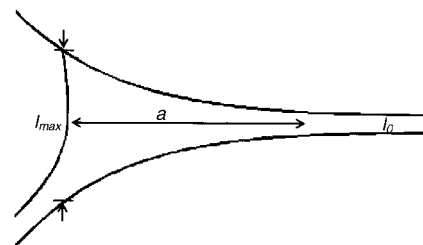


**Figure 12** Schematic of measured parameters used in calculating  $G_{ES}$  stretching.

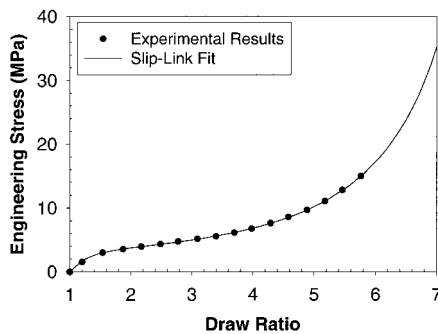


**Figure 13** Engineering stress–strain curves of ES30, used in calculating  $G_{\text{ES stretching}}$ . A slip-link fit has been applied to extrapolate the curve to higher draw ratios.

The calculated strain rate was then applied to a uniaxial tension specimen, and the engineering stress–strain curve was obtained. The ES30 stretching component of  $G$  ( $G_{\text{ES stretching}}$ ) was calculated from the area under the stress–strain curve up to the maximum ES30 draw ratio ( $\lambda_{\text{max}}$ ) and the initial ES30 layer thickness ( $l_0$ ):

$$G_{\text{ES stretching}} = l_0 \int_1^{\lambda_{\text{max}}} \sigma d\lambda \quad (2)$$

For LDPE/ES30 (115/15  $\mu\text{m}$ ) at ambient temperature, a maximum draw ratio at the front of the crack tip ( $\lambda_{\text{max}}$ ) of  $6.25 \pm 0.25$  was measured (from Fig. 5). Unavoidable tilting of the specimen in the SEM tensile stage prevented accurate measurements of the damage zone length due to inaccuracy of the displayed scale. Therefore,  $a$  was measured from *in situ* observation of the damage zone with a telescopic lens video camera. The length of the damage zone was 200  $\mu\text{m}$ , and the calculated engineering strain rate was 16  $\text{min}^{-1}$ .

A simple uniaxial tension stress–strain experiment was performed. Although the stretched ES30 experiences a constrained (pure shear) stress state, a simple uniaxial tension testing geometry can be used because of the similarity in stress–strain response of simple uniaxial tension and pure shear for rubbery and elastomeric materials.<sup>11,12</sup> Elastomeric ES stress–strain curves may be described by an elastic slip-link fit.<sup>13</sup> A stress–strain curve of ES30 at 16  $\text{min}^{-1}$  with a slip-link fit to higher draw ratios was used to calculate  $G_{\text{ES stretching}}$  (Fig. 13). A slip-link fit was necessary most likely because of small differences in the stress state that allowed the ES to be stretched to higher draw ratios. The area under the stress–strain curve to a draw ratio of  $6.25 \pm 0.25$  was  $70 \pm 13 \text{ MJ/m}^3$ . Using eq. (2)  $G_{\text{ES stretching}}$  was  $1000 \pm 200 \text{ J/m}^2$ , about 50% of  $G$  ( $2080 \pm 80 \text{ J/m}^2$ ). Therefore, LDPE deformation sig-

nificantly contributed to  $G$ , most likely on the same scale as the ES30 contribution.

The same measurements and calculations were applied to LDPE/ES40 (120/15  $\mu\text{m}$ ) ( $G = 1600 \text{ J/m}^2$ ). The area under the stress–strain curve to a draw ratio of  $10.5 \pm 0.5$  was  $65 \pm 10 \text{ MJ/m}^3$ , which were then used in eq. (2) to calculate a  $G_{\text{ES stretching}}$  of  $1000 \pm 200 \text{ J/m}^2$ . Similar to LDPE/ES30, LDPE/ES40 showed that  $G_{\text{ES stretching}}$  was 50% of  $G_{\text{measured}}$ .

Beam arm deformation contributions to delamination toughness were also calculated for LDPE/ES30 (90/10). Plastic deformation was evident after peeling because the beam arms did not return to their original positions upon removal of the load and the curvature of the beam arms did not match the elastica prediction.<sup>5,14</sup> Beam arm deformation consists of two components, stretching and bending. The stretching contribution was calculated by correlating the strain of the beam arm during stretching to a stress–strain curve of the microlayer and shown to be within experimental error ( $<3.5\%$  of measured delamination toughness).<sup>15</sup> The bending contribution was assumed to be on the same scale as the stretching correction. Therefore, deformation in both ES30 and LDPE in the damage zone was the major factor that controls delamination toughness.

## CONCLUSIONS

Adhesion between LDPE and ES was highly dependent on styrene content, ES layer thickness, and temperature. As expected, delamination toughness decreased with increasing styrene content in the ES copolymer. A linear correlation between delamination toughness and styrene content predicted that no adhesion would be observed with 72.5 wt % styrene in ES. Delamination toughness scaled approximately with ES layer thickness, which suggested that resistance to delamination was determined by deformation of the entire ES layer. The actual interfacial failure made a negligible contribution. From *in situ* observation of the damage zone in a SEM tensile deformation stage and from analysis of peel fracture surfaces, delamination mechanisms were characterized for both high and low adhesion systems. For high adhesion systems (LDPE/ES30, LDPE/ES40), delamination occurred by stretching and subsequent recovery of the ES layer accompanied by localized stretching and crazing of the polyethylene layer. For low adhesion systems (LDPE/ES60 and LDPE/ES68), a layer thickness effect was observed which indicated similar bulk stretching and recovery of the ES layer with no significant LDPE deformation.

The effect of temperature on delamination toughness for two representative systems was examined and observed to be strongly dependent on the primary ES thermal transitions. Delamination toughness was

highest around the ES  $T_g$  because the most energy was required to develop a damage zone and stretch out the ES layer. For LDPE/ES30, tests below the ES30  $T_g$  were not successful due to yielding or breaking of the beam arms before the crack propagated; however, the LDPE/ES68 system showed a sharp decrease in delamination toughness below the ES68  $T_g$ . This was due to the low interfacial strength and the inability of systems to form a damage zone. When the temperature was increased above the melting or softening point of ES30 and ES68, delamination toughness decreased because the ES was easier to deform. For the higher adhesion LDPE/ES30 system, cohesive failure was observed at 70°C and above because the interface was stronger than the cohesive strength of ES30.

A quantitative description of bulk ES stretching for the two high adhesion systems was made by correlating ES stretching in the damage zone to the ES engineering stress-strain curve. As calculated, the ES stretching contributed about 50% to the measured delamination toughness. The remaining energy was assumed to be due primarily to polyethylene deformation.

The authors thank Dr. Steven P. Chum and Dr. Martin J. Guest of The Dow Chemical Co. for providing technical assistance. The financial support of The Dow Chemical Co. is gratefully acknowledged.

## References

1. Chen, H.; Guest, M. J.; Chum, S.; Hiltner, A.; Baer, E. *J Appl Polym Sci* 1998, 70, 109.
2. Bright, W. M. in *Adhesion and Adhesives*; Clark, J.; Rutzler, A. J. E.; Savage, R. L., Eds., Wiley: New York, 1954, pp. 130–138.
3. Kaelble, D. H. *J Adhes* 1969, 1, 102.
4. Gent, A. N.; Petrich, R. P. *Proc R Soc London Series A* 1969, 310, 433.
5. Ebeling, T.; Hiltner, A.; Baer, E. *J Appl Polym Sci* 1998, 68, 793.
6. Ebeling, T.; Hiltner, A.; Baer, E. *Polymer* 1999, 40, 1525.
7. Ebeling, T.; Hiltner, A.; Baer, E. *Polymer* 1999, 40, 1985.
8. Mueller, C. D.; Nazarenko, S.; Ebeling, T.; Schuman, T. L.; Hiltner, A.; Baer, E. *Polym Eng Sci* 1997, 2, 355.
9. Kinloch, A. J.; Yuen, M. L. *J Adhes* 1989, 30, 151.
10. Kinloch, A. J.; Yuen, M. L. *J Mater Sci* 1989, 24, 2183.
11. Lambert-Diani, J.; Rey, C. *Eur J Mech A Solids* 1999, 18, 1027.
12. Treloar, L. R. G. *Trans Faraday Soc* 1944, 40, 59.
13. Chang, A.; Chum, S. P.; Hiltner, A.; Baer, E. *J Polym Sci Part B: Polym Phys* 2002, 40, 142.
14. Kendall, K. *J Adhes* 1973, 5, 105.
15. Kinloch, A. J.; Lau, C. C.; Williams, J. G. *Int J Fract* 1994, 66, 45.